

2005

Dimer and Trimer Fluctuations in the $s=1/2$ Transverse XX Chain

Oleg Derzhko

Taras Krokhmal'skii

Joachim Stolze

Gerhard Müller

University of Rhode Island, gmuller@uri.edu

Follow this and additional works at: https://digitalcommons.uri.edu/phys_facpubs

Citation/Publisher Attribution

Derzhko, O., Krokhmal'skii, T., Stolze, J., & Müller, G. (2005). Dimer and trimer fluctuations in the $s=1/2$ transverse XX chain. *Physical Review B*, 71(10), 104432. doi: 10.1103/PhysRevB.71.104432
Available at: <http://dx.doi.org/10.1103/PhysRevB.71.104432>

This Article is brought to you by the University of Rhode Island. It has been accepted for inclusion in Physics Faculty Publications by an authorized administrator of DigitalCommons@URI. For more information, please contact digitalcommons-group@uri.edu. For permission to reuse copyrighted content, contact the author directly.

Dimer and Trimer Fluctuations in the $s=1/2$ Transverse XX Chain

Terms of Use

All rights reserved under copyright.

Dimer and trimer fluctuations in the $s=\frac{1}{2}$ transverse XX chain

Oleg Derzhko,^{1,2,*} Taras Krokhmal'skii,¹ Joachim Stolze,³ and Gerhard Müller⁴

¹*Institute for Condensed Matter Physics, National Academy of Sciences of Ukraine, 1 Svientsitskii Street, L'viv-II 79011, Ukraine*

²*Max-Planck-Institut für Physik Komplexer Systeme, Nöthnitzer Straße 38, 01187 Dresden, Germany*

³*Institut für Physik, Universität Dortmund, 44221 Dortmund, Germany*

⁴*Department of Physics, University of Rhode Island, Kingston, Rhode Island 02881-0817, USA*

(Received 10 November 2004; published 31 March 2005)

Exact results for the dynamic dimer and trimer structure factors of the one-dimensional $s=\frac{1}{2}$ XX model in a transverse magnetic field ($\parallel z$) are presented and discussed in relation to known exact results for the dynamic spin structure factors. In the framework of the Jordan-Wigner representation, the accessible spectrum of the dimer fluctuation operator is limited to two-fermion excitations, whereas that of the trimer fluctuation operator involves two- and four-fermion excitations. The spectral boundaries, soft modes, and singularity structure of the four-fermion excitation continuum as probed by the dynamic trimer structure factor are examined and compared to corresponding properties of the two-fermion excitation continuum, as probed by the dynamic dimer and transverse spin structure factors.

DOI: 10.1103/PhysRevB.71.104432

PACS number(s): 75.10.-b

I. INTRODUCTION

The theoretical and computational study of frequency-resolved quantum fluctuations and thermal fluctuations in many-body model systems is an important area of research for several reasons. Such fluctuations are observable directly or indirectly by a host of measuring techniques used in condensed-matter physics and materials science. The shape of the spectrum (dispersions, bandwidths, gaps, soft modes, etc.), the spectral-weight distributions, and the singularity structure of the dynamic structure factors as measured or calculated for specific fluctuation operators yield detailed insights into the state of the material and reveal important clues about the susceptibility of the system to phase transitions with order parameters modeled after the fluctuation operators at hand.¹

An increasing number of exactly solvable quantum many-body model systems turn out to be relevant for situations where certain degrees of freedom of a material are kinematically constrained to one spatial dimension. Many such situations offer the most detailed comparisons in many-body dynamics of exact theoretical results with direct experimental observation.²⁻⁴

Various properties of dynamic spin structure factors of quantum spin chain models are observable in quasi-one-dimensional magnetic insulators, for example, via magnetic neutron scattering.⁵ The properties of dynamic dimer and trimer structure factors, on the other hand, are important indicators of structural phase transitions driven by magnetic interactions, such as in spin-Peierls compounds. Dimer fluctuations are key participants in phonon-assisted optical absorption processes of magnetic chain compounds and are thus observable in optical conductivity measurements.⁶⁻¹⁰

Here we consider the exactly solvable $s=\frac{1}{2}$ XX chain with a magnetic field in the direction transverse to the spin coupling (in spin space).^{11,12} The Hamiltonian reads

$$H = \sum_{n=1}^N \Omega s_n^z + \sum_{n=1}^N J (s_n^x s_{n+1}^x + s_n^y s_{n+1}^y). \quad (1.1)$$

We set $g\mu_B=1$, $\hbar=1$, use the exchange constant as the energy unit, and measure the magnetic field Ω in units of J . The Jordan-Wigner transformation to spinless lattice fermions maintains the bilinear operator structure,

$$H = \sum_{n=1}^N \Omega \left(c_n^\dagger c_n - \frac{1}{2} \right) + \frac{1}{2} \sum_{n=1}^N J (c_n^\dagger c_{n+1} - c_n c_{n+1}^\dagger). \quad (1.2)$$

A Fourier transform, $c_\kappa = N^{-1/2} \sum_{n=1}^N \exp(i\kappa n) c_n$, brings (1.2) into diagonal form

$$H = \sum_{\kappa} \Lambda_{\kappa} \left(c_{\kappa}^{\dagger} c_{\kappa} - \frac{1}{2} \right), \quad \Lambda_{\kappa} = \Omega + J \cos \kappa. \quad (1.3)$$

For periodic boundary conditions in (1.1) the allowed values of the fermion momenta κ_i depend on whether the number N_f of fermions in the system is even or odd: $\kappa_i \in \{(2\pi/N)(n + \frac{1}{2})\}$ if N_f is even or $\kappa_i \in \{(2\pi/N)n\}$ if N_f is odd. Fermion momenta within the first Brillouin zone are specified by integers $n = -N/2, -N/2+1, \dots, N/2-1$ (if N is even) or $n = -(N-1)/2, -(N-1)/2+1, \dots, (N-1)/2$ (if N is odd). The Fermi level in the band Λ_{κ} is controlled by the magnetic field Ω . The number of fermions can vary between an empty band ($N_f=0$) and a full band ($N_f=N$) and is related to the quantum number S^z (the z component of the total spin) of the same model in the spin representation: $S^z = N_f - N/2$.

The dimer and trimer fluctuation operators for the XX model (1.1) will be introduced in Sec. II. The two- and four-fermion dynamic structure factors associated with these fluctuation operators will be discussed in Secs. III and IV, respectively. Finally, in Sec. V we give the conclusions and perspectives for future work.

II. FLUCTUATION OPERATORS AND DYNAMIC STRUCTURE FACTORS

Most fluctuation operators of interest are constructed from local operators A_n of the model system under consideration

$$A_\kappa = \frac{1}{\sqrt{N}} \sum_{n=1}^N \exp(i\kappa n) A_n. \quad (2.1)$$

Associated with each fluctuation operator (2.1) is a dynamic structure factor,

$$S_{AA}(\kappa, \omega) = 2\pi \sum_{\lambda\lambda'} \frac{\exp(-\beta E_{\lambda'})}{Z} |\langle \lambda' | A_\kappa | \lambda \rangle|^2 \delta(\omega - E_\lambda + E_{\lambda'}), \quad (2.2)$$

which describes fluctuations of a specific kind. Here E_λ and $|\lambda\rangle$ are the eigenvalues and the eigenvectors of H , and Z is the partition function. Of particular interest is the zero-temperature limit $T=0$ (i.e., $\beta \rightarrow \infty$), where the thermal fluctuations fade away leaving pure quantum fluctuations in the wake. What remains in (2.2) are transitions between the ground state and all excited states that can be reached by the fluctuation operator A_κ

$$S_{AA}(\kappa, \omega) \stackrel{(\beta \rightarrow \infty)}{=} 2\pi \sum_{\lambda} |\langle \text{GS} | A_\kappa | \lambda \rangle|^2 \delta(\omega - \omega_\lambda), \quad \omega_\lambda = E_\lambda - E_{\text{GS}}. \quad (2.3)$$

The dynamically relevant spectrum observable in (2.2) or (2.3) may vary considerably between fluctuation operators. Among other things, the spectrum is sensitive to their symmetry properties.

For the $s=\frac{1}{2}$ transverse XX chain (1.1), the most important and most widely studied dynamic structure factors are those for the local spin operators

$$s_n^z = c_n^\dagger c_n - \frac{1}{2}, \quad s_n^+ = s_n^x + i s_n^y = c_n^\dagger \exp\left(i\pi \sum_{j=1}^{n-1} c_j^\dagger c_j\right),$$

$$s_n^- = s_n^x - i s_n^y = \exp\left(-i\pi \sum_{j=1}^{n-1} c_j^\dagger c_j\right) c_n. \quad (2.4)$$

At zero temperature the dynamic spin structure factor $S_{zz}(\kappa, \omega)$ is known to couple exclusively to the continuum of particle-hole excitations in the fermion representation, whereas $S_{xx}(\kappa, \omega) = S_{yy}(\kappa, \omega)$ couples to excitations involving an arbitrarily high number of fermion excitations from the ground state.^{13,14}

The fluctuation operators considered here are constructed from local spin operators on nearest and next-nearest neighbor sites. The dimer fluctuation operator D_κ and trimer fluctuation operator T_κ are obtained via (2.1) from

$$D_n = s_n^x s_{n+1}^x + s_n^y s_{n+1}^y = \frac{1}{2} (c_n^\dagger c_{n+1} - c_n c_{n+1}^\dagger) \quad (2.5)$$

and

$$T_n = s_n^x s_{n+2}^x + s_n^y s_{n+2}^y$$

$$= \frac{1}{2} (c_n^\dagger c_{n+2} - c_n c_{n+2}^\dagger - 2c_n^\dagger c_{n+1}^\dagger c_{n+1} c_{n+2} + 2c_n c_{n+1}^\dagger c_{n+1} c_{n+2}^\dagger), \quad (2.6)$$

respectively. There is no unique way of defining dimer and trimer fluctuation operators. The most suitable choice depends on the nature and symmetry of the model system at hand. The operators (2.5) and (2.6) have the advantage that the associated dynamic structure factors $S_{DD}(\kappa, \omega)$ and $S_{TT}(\kappa, \omega)$ can be analyzed exactly for the $s=\frac{1}{2}$ transverse XX chain (1.1) in the fermion representation.

As a motivation for the dimer and trimer operators used in this study, we offer a twofold argument. For a completely dimerized state, where nearest-neighbor spin correlations alternate between zero and a nonzero value along the chain, the operator \sqrt{ND}_π plays the role of dimer-order parameter. Likewise, for a completely trimerized state, where next-nearest neighbor spin correlations assume a period-three sequence of values zero, zero, nonzero, the operator $\sqrt{NT}_{2\pi/3}$ plays the role of trimer-order parameter.

Conversely, if we perturb the uniform XX Hamiltonian (1.1) by interactions of the form

$$H_D = \varepsilon \sum_{n=1}^N \cos(\pi n) D_n \quad (2.7)$$

or

$$H_T = \varepsilon \sum_{n=1}^N \cos\left(\frac{2\pi n}{3}\right) T_n, \quad (2.8)$$

the ground state becomes dimerized or trimerized, respectively. In the former case, nearest-neighbor correlations are modified by period-two perturbative corrections of order $-\varepsilon$, $+\varepsilon$ and in the latter case by period-three corrections of order $-\frac{1}{2}\varepsilon$, $-\frac{1}{2}\varepsilon$, $+\varepsilon$.

We may formally introduce the polymer fluctuation operator of order l , $\mathcal{P}_\kappa^{(l)}$, via (2.1) from

$$\mathcal{P}_n^{(l)} = s_n^x s_{n+l}^x + s_n^y s_{n+l}^y. \quad (2.9)$$

It includes the dimer and trimer operators for $l=1,2$, respectively: $\mathcal{P}_n^{(1)} = D_n$, $\mathcal{P}_n^{(2)} = T_n$. From the fermion representation of the polymer operator (2.9) as carried out explicitly in (2.5) and (2.6) for the lowest two orders, it is evident that the dynamic polymer structure factor $S_{\mathcal{P}\mathcal{P}}(\kappa, \omega)$ at zero temperature will involve $2m$ -fermion excitations with $m=1,2,\dots,l$ from the ground state. For an infinitely long chain ($N \rightarrow \infty$) the polymer fluctuation operator and the function $S_{\mathcal{P}\mathcal{P}}(\kappa, \omega)$ may thus serve useful roles in attempts to understand the enormously complex dynamic spin structure factors $S_{xx}(\kappa, \omega) = S_{yy}(\kappa, \omega)$. Such tools by which the complexity of the dynamically relevant excitation spectrum can be gradually and systematically increased are not only useful for the calculations in the fermion representation as performed here but also for the recently developed techniques of calculating transition rates for the XX model in the framework of the Bethe ansatz.¹⁵⁻¹⁷ The time-dependent polymer correlation

function is related, in the limit $l \rightarrow \infty$, to time-dependent spin correlation functions as follows:

$$\langle \mathcal{P}_n^{(l)}(t) \mathcal{P}_{n+m}^{(l)}(0) \rangle \xrightarrow{(l \rightarrow \infty)} 2 \langle s_n^x(t) s_{n+m}^x(0) \rangle^2 + 2 \langle s_n^y(t) s_{n+m}^y(0) \rangle^2. \quad (2.10)$$

Note that $\langle s_n^x(t) s_{n+m}^y(0) \rangle$ is nonzero only if $\Omega \neq 0$.

III. TWO-FERMION DYNAMIC STRUCTURE FACTORS

We start with the dynamic quantities, which are governed by particle-hole excitations. The equilibrium time-dependent correlation functions for the operators $s_n^z(t)$ and $D_n(t)$ can be evaluated directly

$$\begin{aligned} & \langle s_n^z(t) s_{n+l}^z(0) \rangle - \langle s^z \rangle^2 \\ &= \frac{1}{N^2} \sum_{\kappa_1, \kappa_2} e^{-i(\kappa_1 - \kappa_2)t} \exp[i(\Lambda_{\kappa_1} - \Lambda_{\kappa_2})t] n_{\kappa_1} (1 - n_{\kappa_2}), \end{aligned} \quad (3.1)$$

$$\begin{aligned} & \langle D_n(t) D_{n+l}(0) \rangle - \langle D \rangle^2 \\ &= \frac{1}{N^2} \sum_{\kappa_1, \kappa_2} \cos^2 \frac{\kappa_1 + \kappa_2}{2} e^{-i(\kappa_1 - \kappa_2)t} \\ & \quad \times \exp[i(\Lambda_{\kappa_1} - \Lambda_{\kappa_2})t] n_{\kappa_1} (1 - n_{\kappa_2}), \end{aligned} \quad (3.2)$$

where $n_\kappa = 1/[1 + \exp(\beta\Lambda_\kappa)]$ is the Fermi function and

$$\langle s^z \rangle = \frac{1}{N} \sum_{n=1}^N \langle s_n^z \rangle = -\frac{1}{2N} \sum_{\kappa} \tanh \frac{\beta\Lambda_\kappa}{2}, \quad (3.3)$$

$$\langle D \rangle = \frac{1}{N} \sum_{n=1}^N \langle D_n \rangle = -\frac{1}{2N} \sum_{\kappa} \cos \kappa \tanh \frac{\beta\Lambda_\kappa}{2}. \quad (3.4)$$

The associated dynamic structure factors,

$$\begin{aligned} S_{AA}(\kappa, \omega) &= \sum_{l=1}^N \exp(-i\kappa l) \int_{-\infty}^{\infty} dt \exp(i\omega t) \\ & \quad \times \langle (A_n(t) - \langle A \rangle)(A_{n+l}(0) - \langle A \rangle) \rangle, \end{aligned} \quad (3.5)$$

all of which involve two-fermion transitions, are obtained by Fourier transform. The resulting expressions for $N \rightarrow \infty$ can be brought into the form

$$\begin{aligned} S_{zz}(\kappa, \omega) &= \int_{-\pi}^{\pi} d\kappa_1 n_{\kappa_1} (1 - n_{\kappa_1 + \kappa}) \delta(\omega + \Lambda_{\kappa_1} - \Lambda_{\kappa_1 + \kappa}) \\ &= \sum_{\kappa^*} \frac{n_{\kappa^*} (1 - n_{\kappa + \kappa^*})}{2 \left| J \sin \frac{\kappa}{2} \cos \left(\frac{\kappa}{2} + \kappa^* \right) \right|}, \end{aligned} \quad (3.6)$$

$$S_{DD}(\kappa, \omega) = \sum_{\kappa^*} \frac{\cos^2 \left(\frac{\kappa}{2} + \kappa^* \right) n_{\kappa^*} (1 - n_{\kappa + \kappa^*})}{2 \left| J \sin \frac{\kappa}{2} \cos \left(\frac{\kappa}{2} + \kappa^* \right) \right|}, \quad (3.7)$$

where $-\pi \leq \kappa^* \leq \pi$ are the solutions of the equation

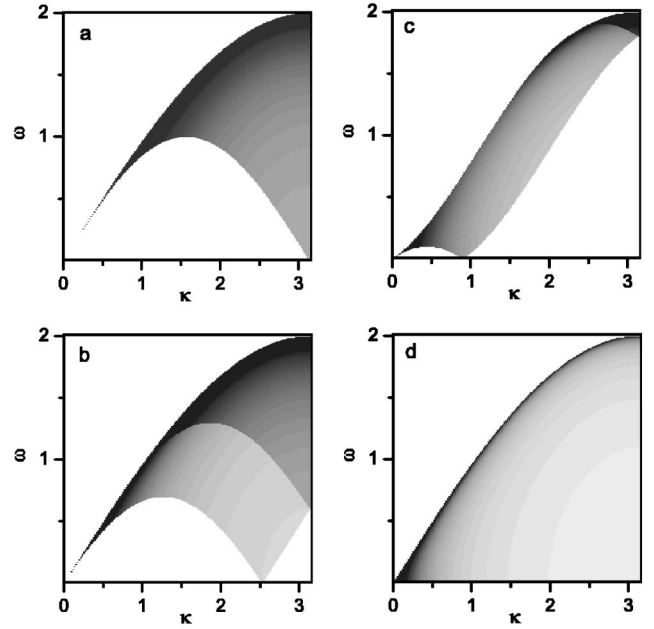


FIG. 1. $S_{zz}(\kappa, \omega)$ at $T=0$ and (a) $\Omega=0$, (b) $\Omega=0.3$, (c) $\Omega=0.9$, and (d) at $T \rightarrow \infty$ (independent of Ω ; only $\omega \geq 0$ is shown).

$$\omega = -2J \sin \frac{\kappa}{2} \sin \left(\frac{\kappa}{2} + \kappa^* \right). \quad (3.8)$$

The dynamic structure factors (3.6) and (3.7) are governed by the two-fermion (particle-hole) excitation continuum, the properties of which were examined in Refs. 18 and 19. This continuum is well visible in Figs. 1 and 2. At zero temperature, $T=0$, the two-fermion excitation continuum has the following lower, middle and upper boundaries in the (κ, ω) -plane (we assume that $0 \leq \kappa \leq \pi$ in the rest of the equations of this section; these equations are valid also for $-\pi \leq \kappa \leq 0$ after the change $\kappa \rightarrow -\kappa$)

$$\frac{\omega_l}{|J|} = 2 \sin \frac{\kappa}{2} \left| \sin \left(\frac{\kappa}{2} - \alpha \right) \right|, \quad (3.9)$$

$$\frac{\omega_m}{|J|} = 2 \sin \frac{\kappa}{2} \sin \left(\frac{\kappa}{2} + \alpha \right), \quad (3.10)$$

$$\frac{\omega_u}{|J|} = \begin{cases} 2 \sin \frac{\kappa}{2} \sin \left(\frac{\kappa}{2} + \alpha \right), & \text{if } 0 \leq \kappa \leq \pi - 2\alpha, \\ 2 \sin \frac{\kappa}{2}, & \text{if } \pi - 2\alpha \leq \kappa \leq \pi, \end{cases} \quad (3.11)$$

respectively. The parameter $\alpha = \arccos(\Omega/|J|)$ varies from π

when $\Omega = -|J|$ to 0 when $\Omega = |J|$. The ω profiles at fixed κ of the two-fermion dynamic structure factors may exhibit square-root divergences (a common density-of-states effect in one dimension) when $\omega \rightarrow 2|J|\sin(\kappa/2)$. At $T > 0$ the lower boundary of two-fermion excitation continuum is smeared

out. The spectral weight in (3.6) and (3.7) is now confined to $|\omega| \leq 2|J|\sin(\kappa/2)$.

Closed-form expressions for the two-fermion dynamic structure factors (3.6) and (3.7) exist in the low- and high-temperature limits. At $T=0$ we have

$$S_{zz}(\kappa, \omega) = \frac{1}{\sqrt{4J^2 \sin^2 \frac{\kappa}{2} - \omega^2}} \cdot \begin{cases} \Theta(\omega - \omega_l)\Theta(\omega_u - \omega), & \text{if } 0 \leq \kappa \leq \pi - 2\alpha, \\ [\Theta(\omega - \omega_l) + \Theta(\omega - \omega_m)]\Theta(\omega_u - \omega), & \text{if } \pi - 2\alpha \leq \kappa \leq \pi, \end{cases} \quad (3.12)$$

$$S_{DD}(\kappa, \omega) = \frac{\sqrt{4J^2 \sin^2 \frac{\kappa}{2} - \omega^2}}{4J^2 \sin^2 \frac{\kappa}{2}} \cdot \begin{cases} \Theta(\omega - \omega_l)\Theta(\omega_u - \omega), & \text{if } 0 \leq \kappa \leq \pi - 2\alpha, \\ [\Theta(\omega - \omega_l) + \Theta(\omega - \omega_m)]\Theta(\omega_u - \omega), & \text{if } \pi - 2\alpha \leq \kappa \leq \pi, \end{cases} \quad (3.13)$$

and at $T \rightarrow \infty$ we have

$$S_{zz}(\kappa, \omega) = \frac{1}{2\sqrt{4J^2 \sin^2 \frac{\kappa}{2} - \omega^2}} \Theta\left(2|J|\sin \frac{\kappa}{2} - |\omega|\right), \quad (3.14)$$

$$S_{DD}(\kappa, \omega) = \frac{\sqrt{4J^2 \sin^2 \frac{\kappa}{2} - \omega^2}}{8J^2 \sin^2 \frac{\kappa}{2}} \Theta\left(2|J|\sin \frac{\kappa}{2} - |\omega|\right). \quad (3.15)$$

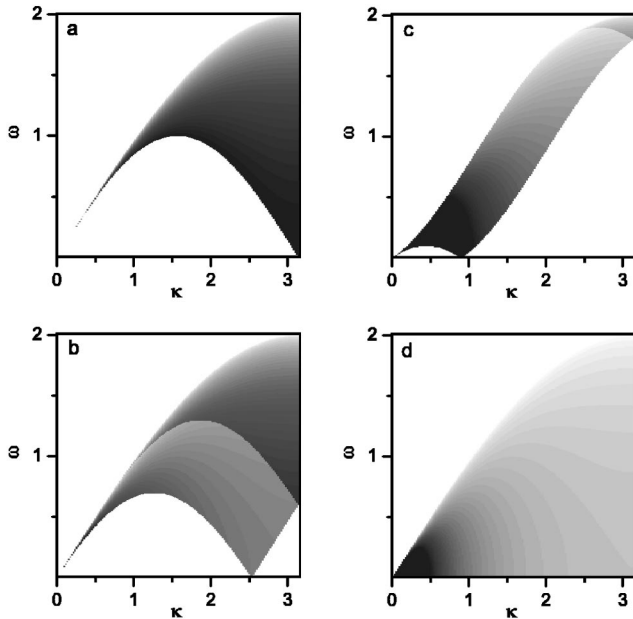


FIG. 2. $S_{DD}(\kappa, \omega)$ at $T=0$ and (a) $\Omega=0$, (b) $\Omega=0.3$, (c) $\Omega=0.9$, and (d) at $T \rightarrow \infty$ (independent of Ω ; only $\omega \geq 0$ is shown).

The zero-temperature results for $S_{zz}(\kappa, \omega)$ can be found in Eq. (2.3) of Ref. 18 and for $S_{DD}(\kappa, \omega)$ at $\Omega=0$ in Eq. (3.2) of Ref. 8.

In Figs. 1 and 2 we show the dynamic structure factors (3.6) and (3.7) at zero temperature $T=0$ and different values of the transverse field [Figs. 1(a)–1(c) and 2(a)–2(c)], and at $T \rightarrow \infty$ [Figs. 1(d) and 2(d)]. The results for $T \rightarrow \infty$ are independent of Ω . As we can see, the two-fermion dynamic structure factors are nonzero within the two-fermion excitation continuum in the (κ, ω) plane. Their spectral-weight distributions are controlled by the Fermi functions, the multiplicity of the solution of Eq. (3.8), the singularities in the density of one-particle states, and the explicit form of the rest of the integrand in (3.6) and (3.7). Another two-fermion dynamic quantity will be presented in Sec. IV, namely, the two-fermion contribution to the dynamic trimer structure factor, $S_{TT}^{(2)}(\kappa, \omega)$.

IV. FOUR-FERMION DYNAMIC STRUCTURE FACTOR

Next we consider the dynamics of the trimer fluctuations. The method remains the same but its execution is more tedious. In addition to two-fermion transitions also four-fermion transitions contribute to the trimer fluctuations. The expression for the equilibrium time-dependent trimer-trimer correlation function reads

$$\begin{aligned} & \langle T_n(t) T_{n+l}(0) \rangle - \langle T \rangle^2 \\ &= \frac{1}{N^2} \sum_{\kappa_1, \kappa_2} C^{(2)}(\kappa_1, \kappa_2) e^{-i(\kappa_1 - \kappa_2)l} \exp[i(\Lambda_{\kappa_1} - \Lambda_{\kappa_2})t] \\ & \times n_{\kappa_1} (1 - n_{\kappa_2}) + \frac{1}{N^4} \sum_{\kappa_1, \kappa_2, \kappa_3, \kappa_4} C^{(4)}(\kappa_1, \kappa_2, \kappa_3, \kappa_4) \\ & \times e^{-i(\kappa_1 + \kappa_2 - \kappa_3 - \kappa_4)l} \exp[i(\Lambda_{\kappa_1} + \Lambda_{\kappa_2} - \Lambda_{\kappa_3} - \Lambda_{\kappa_4})t] \\ & \times n_{\kappa_1} n_{\kappa_2} (1 - n_{\kappa_3}) (1 - n_{\kappa_4}), \end{aligned} \quad (4.1)$$

where

$$\langle T \rangle = \frac{1}{N} \sum_{n=1}^N \langle T_n \rangle = c_2 + 2c_1^2 - 2c_0c_2, \quad (4.2)$$

$$\begin{aligned} C^{(2)}(\kappa_1, \kappa_2) &= (1 - 2c_0)^2 \cos^2(\kappa_1 + \kappa_2) + 4c_1(1 - 2c_0) \\ &\times \left[\cos^2\left(\kappa_1 + \frac{\kappa_2}{2}\right) + \cos^2\left(\frac{\kappa_1}{2} + \kappa_2\right) \right] \\ &+ 4c_1^2(\cos^2 \kappa_1 + \cos^2 \kappa_2) + 8(-c_2 + c_1^2 + 2c_0c_2) \\ &\times \cos^2 \frac{\kappa_1 + \kappa_2}{2} + 8c_1^2 \cos^2 \frac{\kappa_1 - \kappa_2}{2} \\ &+ 4c_1(1 - 2c_0 - 4c_2) \left(\cos^2 \frac{\kappa_1}{2} + \cos^2 \frac{\kappa_2}{2} \right) + 4c_2 \\ &- 8c_1 - 8c_1^2 + 4c_2^2 + 16c_0c_1 - 8c_0c_2 + 16c_1c_2, \end{aligned} \quad (4.3)$$

$$\begin{aligned} C^{(4)}(\kappa_1, \kappa_2, \kappa_3, \kappa_4) &= 16 \sin^2 \frac{\kappa_1 - \kappa_2}{2} \sin^2 \frac{\kappa_3 - \kappa_4}{2} \\ &\times \cos^2 \frac{\kappa_1 + \kappa_2 + \kappa_3 + \kappa_4}{2}. \end{aligned} \quad (4.4)$$

Here we have introduced the function $c_p = (1/N) \sum_{\kappa} \cos(p\kappa) n_{\kappa}$. For $N \rightarrow \infty$ and at zero temperature we have $c_0 = 1$ if $\Omega \leq -|J|$, $c_0 = \alpha/\pi$ if $-|J| \leq \Omega \leq |J|$, $c_0 = 0$ if $|J| \leq \Omega$, $c_p = (-\text{sgn}(J))^p \sin(p\alpha)/(p\pi)$ if $|\Omega| \leq |J|$ and $c_p = 0$ otherwise ($p = 1, 2, \dots$). At $T \rightarrow \infty$ we have $c_p = \frac{1}{2} \delta_{p,0}$. The resulting dynamic trimer structure factor (3.5) for $N \rightarrow \infty$ then has the following form:

$$S_{TT}(\kappa, \omega) = S_{TT}^{(2)}(\kappa, \omega) + S_{TT}^{(4)}(\kappa, \omega), \quad (4.5)$$

where

$$\begin{aligned} S_{TT}^{(2)}(\kappa, \omega) &= \int_{-\pi}^{\pi} d\kappa_1 C^{(2)}(\kappa_1, \kappa_1 + \kappa) n_{\kappa_1} (1 - n_{\kappa_1 + \kappa}) \\ &\times \delta(\omega + \Lambda_{\kappa_1} - \Lambda_{\kappa_1 + \kappa}), \end{aligned} \quad (4.6)$$

$$\begin{aligned} S_{TT}^{(4)}(\kappa, \omega) &= \frac{1}{4\pi^2} \int_{-\pi}^{\pi} d\kappa_1 \int_{-\pi}^{\pi} d\kappa_2 \int d\kappa_3 C^{(4)}(\kappa_1, \kappa_2, \kappa_3, \kappa_1 + \kappa_2 \\ &- \kappa_3 + \kappa) n_{\kappa_1} n_{\kappa_2} (1 - n_{\kappa_3}) (1 - n_{\kappa_1 + \kappa_2 - \kappa_3 + \kappa}) \\ &\times \delta(\omega + \Lambda_{\kappa_1} + \Lambda_{\kappa_2} - \Lambda_{\kappa_3} - \Lambda_{\kappa_1 + \kappa_2 - \kappa_3 + \kappa}). \end{aligned} \quad (4.7)$$

The spectral weight in this quantity comes from both the two-fermion (one particle and one hole) excitation continuum and the four-fermion (two particles and two holes) excitation continuum. Let us first discuss the properties of the four-fermion excitation continuum and then the properties of $S_{TT}(\kappa, \omega)$. At $T=0$ the four-fermion excitation continuum (for $J = -|J| < 0$) is determined by the conditions

$$\frac{\omega}{|J|} = \cos \kappa_1 + \cos \kappa_2 - \cos \kappa_3 - \cos \kappa_4,$$

$$\begin{aligned} \kappa &= -\kappa_1 - \kappa_2 + \kappa_3 + \kappa_4 [\text{mod}(2\pi)], \quad \cos \kappa_1 \geq \frac{\Omega}{|J|}, \\ \cos \kappa_2 &\geq \frac{\Omega}{|J|}, \quad \cos \kappa_3 \leq \frac{\Omega}{|J|}, \quad \cos \kappa_4 \leq \frac{\Omega}{|J|}, \end{aligned} \quad (4.8)$$

$-\pi \leq \kappa_{1,2,3} \leq \pi$, $-\pi \leq \kappa \leq \pi$. Equations (4.8) imply that the four-fermion excitation continuum (like the two-fermion excitation continuum) exists only if the magnetic field does not exceed the saturation field: $|\Omega| \leq |J|$.

An analytical expression for the lower boundary of the four-fermion excitation continuum in the (κ, ω) plane depends on Ω and κ and is given by one of the following expressions (see the Appendix for additional details):

$$\frac{\omega_l^{(1)}}{|J|} = 2 \sin \frac{|\kappa|}{2} \sin \left(\alpha - \frac{|\kappa|}{2} \right), \quad (4.9)$$

$$\frac{\omega_l^{(2)}}{|J|} = 4 \cos \frac{\kappa}{4} \cos \left(\alpha + \frac{|\kappa|}{4} \right), \quad (4.10)$$

$$\frac{\omega_l^{(3)}}{|J|} = -2 \sin \left(\alpha + \frac{|\kappa|}{2} \right) \sin \left(2\alpha + \frac{|\kappa|}{2} \right), \quad (4.11)$$

$$\frac{\omega_l^{(4)}}{|J|} = -2 \sin \left(\alpha - \frac{|\kappa|}{2} \right) \sin \left(2\alpha - \frac{|\kappa|}{2} \right), \quad (4.12)$$

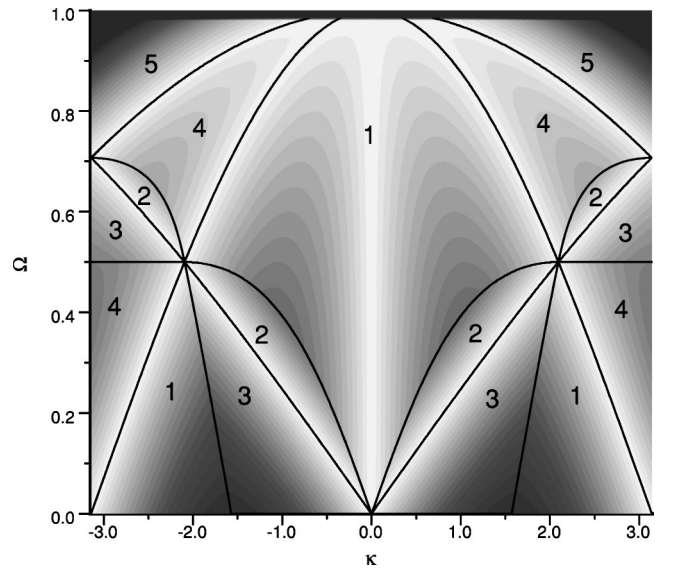


FIG. 3. Lower boundary $\omega_l = \min(\omega_l^{(j)})$, $j = 1, \dots, 5$ of the four-fermion excitation continuum vs wave number κ and transverse field Ω (for $|J|=1$).

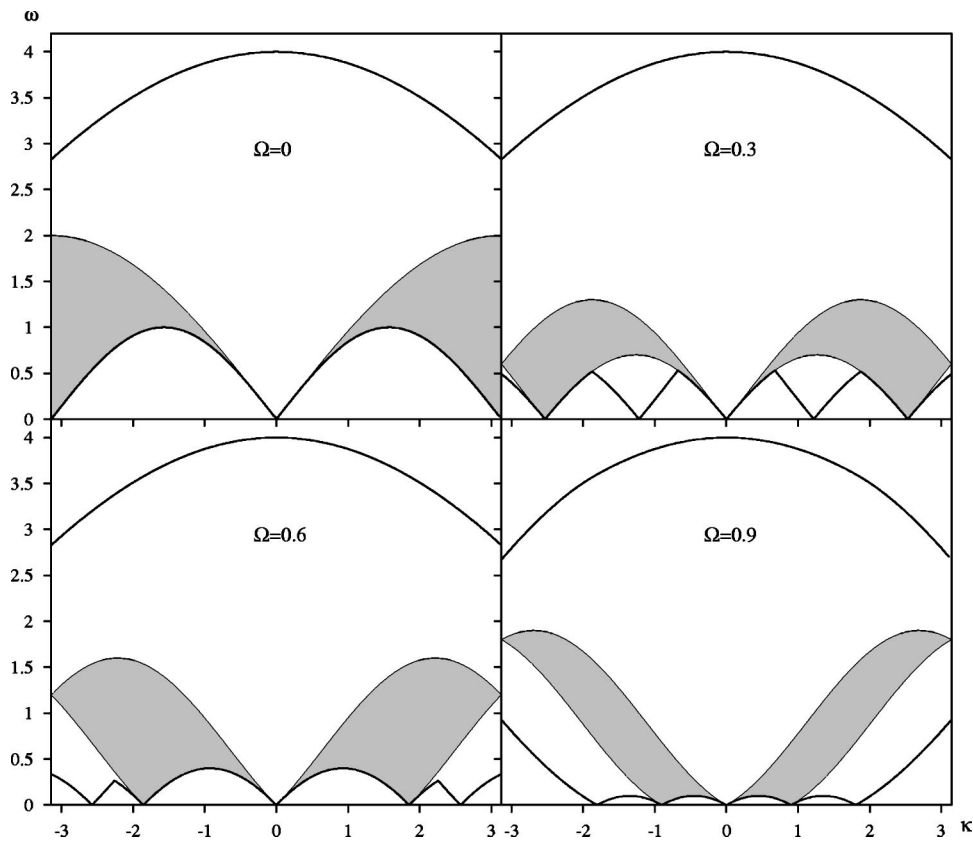


FIG. 4. Lower and upper boundaries of the two- and four-fermion continua for $|J|=1$ and $\Omega=0, 0.3, 0.6,$ and 0.9 . The two-fermion continuum is shown shaded.

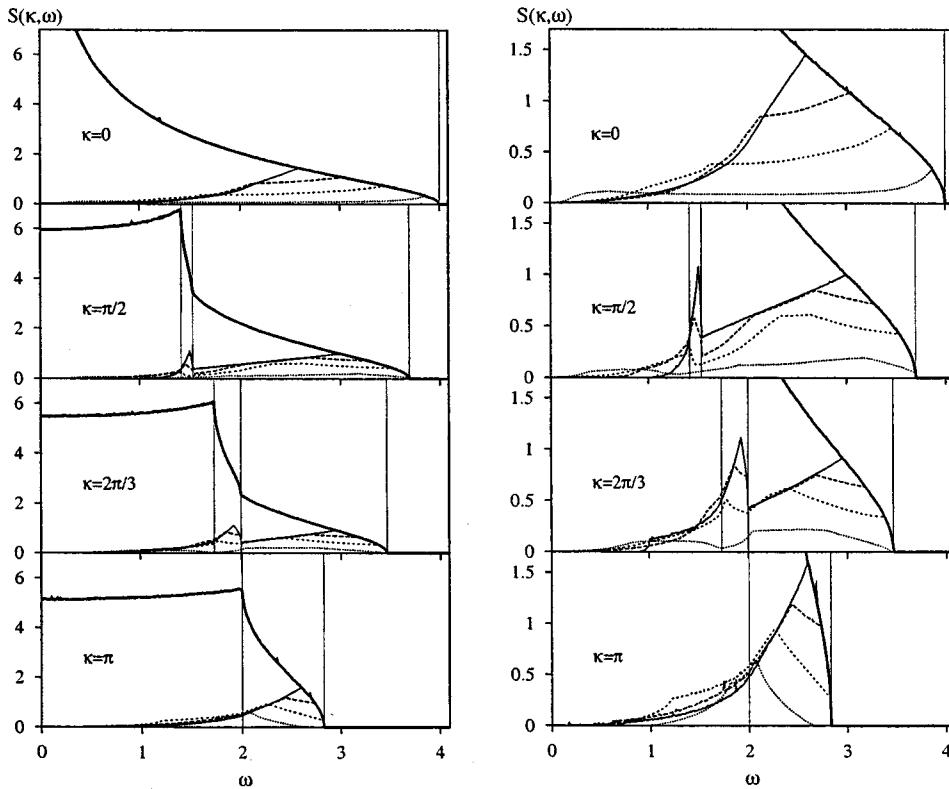


FIG. 5. $S(\kappa, \omega)$ as given in (4.28) vs ω at $\kappa=0, \pi/2, 2\pi/3, \pi$ with $S(\kappa_1, \kappa_2, \kappa_3, \kappa)=1$ (bold curves), and $S(\kappa_1, \kappa_2, \kappa_3, \kappa) = n_{\kappa_1} n_{\kappa_2} (1 - n_{\kappa_3}) (1 - n_{\kappa_1 + \kappa_2 - \kappa_3 + \kappa})$ for $\Omega=0$ (solid curves), $\Omega=0.3$ (long-dashed curves), $\Omega=0.6$ (short-dashed curves), $\Omega=0.9$ (dotted curves). Vertical lines mark the values of $\omega_j^{(j)}$, $j=1, 2, 3$ as given in (4.25)–(4.27). Note the different vertical scales left and right.

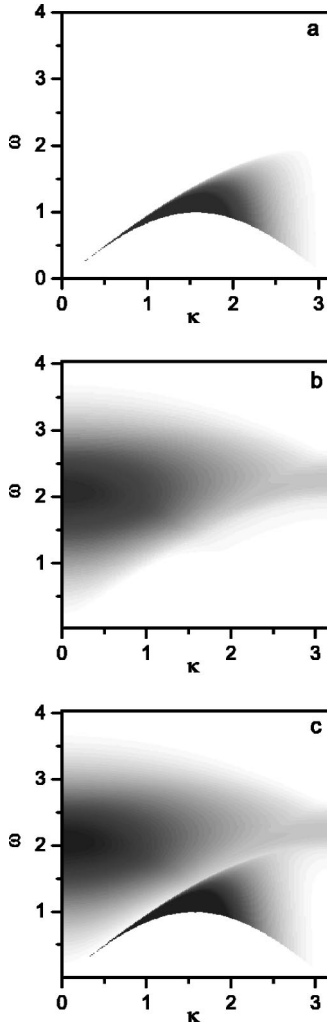


FIG. 6. $S_{TT}(\kappa, \omega)$ at $T=0$ and $\Omega=0$. Separate plots are shown for (a) $S_{TT}^{(2)}(\kappa, \omega)$, (b) $S_{TT}^{(4)}(\kappa, \omega)$, and (c) the sum $S_{TT}(\kappa, \omega)$.

$$\frac{\omega_l^{(5)}}{|J|} = -4 \sin \frac{|\kappa|}{4} \sin \left(\alpha - \frac{|\kappa|}{4} \right). \quad (4.13)$$

The range in κ over which for a given Ω one of the expressions (4.9)–(4.13) forms the lower boundary of the four-fermion continuum can be read off Fig. 3. The darkness in this gray-scale plot is a measure of the size of the energy threshold of the four-fermion continuum (white means zero excitation energy, i.e., a soft mode). The boundary between the region i (where $\omega_l^{(i)}$ is the lower boundary) and the region j (where $\omega_l^{(j)}$ is the lower boundary) follows from the matching condition $\omega_l^{(i)} = \omega_l^{(j)}$ and is given by the formula $|\kappa| = l_{ij}(\alpha)$ where

$$l_{12}(\alpha) = 4 \arctan \frac{\tan \alpha - \sqrt{\tan^2 \alpha - 3}}{3}, \quad |\kappa| \leq \frac{2\pi}{3}, \quad (4.14)$$

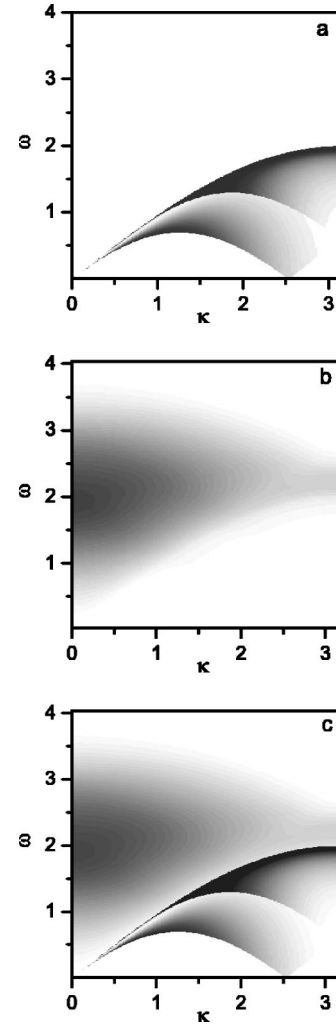


FIG. 7. $S_{TT}(\kappa, \omega)$ at $T=0$ and $\Omega=0.3$. Separate plots are shown for (a) $S_{TT}^{(2)}(\kappa, \omega)$, (b) $S_{TT}^{(4)}(\kappa, \omega)$, and (c) the sum $S_{TT}(\kappa, \omega)$.

$$l_{13}(\alpha) = \pi - \alpha, \quad \frac{\pi}{2} \leq |\kappa| \leq \frac{2\pi}{3}, \quad (4.15)$$

$$l_{14}(\alpha) = 2\alpha, \quad (4.16)$$

$$l_{23}(\alpha) = 2\pi - 4\alpha, \quad (4.17)$$

$$l_{34}(\alpha) = |\kappa| + \cos \alpha - \frac{1}{2}, \quad \frac{2\pi}{3} \leq |\kappa| \leq \pi, \quad (4.18)$$

$$l_{45}(\alpha) = 4\alpha. \quad (4.19)$$

The boundary between regions 2 and 4 is determined by the cubic equation

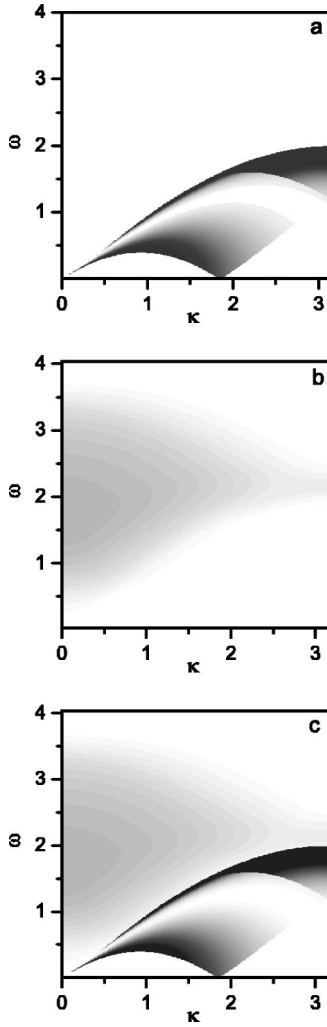


FIG. 8. $S_{TT}(\kappa, \omega)$ at $T=0$ and $\Omega=0.6$. Separate plots are shown for (a) $S_{TT}^{(2)}(\kappa, \omega)$, (b) $S_{TT}^{(4)}(\kappa, \omega)$, and (c) the sum $S_{TT}(\kappa, \omega)$.

$$\begin{aligned} & \left(\sin|\kappa| - 2 \sin \frac{|\kappa|}{2} \right) \tan^3 \alpha + \left(3 + 2 \cos \frac{\kappa}{2} + 3 \cos \kappa \right) \tan^2 \alpha \\ & - \left(2 \sin \frac{|\kappa|}{2} + 3 \sin|\kappa| \right) \tan \alpha + 3 + 2 \cos \frac{\kappa}{2} - \cos \kappa = 0. \end{aligned} \quad (4.20)$$

Typical lower boundaries of the four-fermion continuum for several values of Ω can be seen in Fig. 4. The soft modes according to (4.9)–(4.13) are given by

$$|\kappa_0| = \{0, 2\pi - 4\alpha, 2\alpha, 4\alpha\}. \quad (4.21)$$

Alternatively, the soft modes (4.21) may be determined directly from (4.8). They occur when $\cos \kappa_1 = \cos \kappa_2 = \cos \kappa_3 = \cos \kappa_4 = \cos \alpha$.

The upper boundary of the four-fermion continuum for $0 \leq \Omega \leq |J|/\sqrt{2}$ is given by

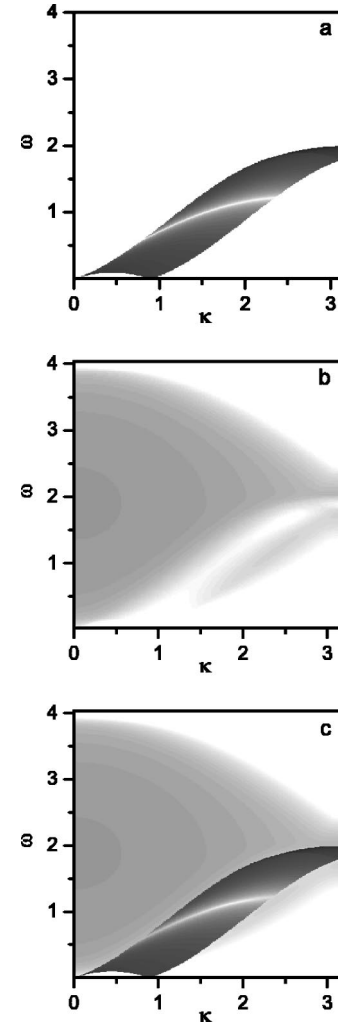


FIG. 9. $S_{TT}(\kappa, \omega)$ at $T=0$ and $\Omega=0.9$. Separate plots are shown for (a) $S_{TT}^{(2)}(\kappa, \omega)$, (b) $S_{TT}^{(4)}(\kappa, \omega)$, and (c) the sum $S_{TT}(\kappa, \omega)$.

$$\frac{\omega_u^{(1)}}{|J|} = 4 \cos \frac{\kappa}{4}. \quad (4.22)$$

For $|J|/\sqrt{2} \leq \Omega \leq |J|$ the upper boundary is given by (4.22) only if $|\kappa| \leq 4\alpha$, whereas, if $4\alpha \leq |\kappa| \leq \pi$, it is given by

$$\frac{\omega_u^{(2)}}{|J|} = 4 \cos \frac{\kappa}{4} \cos \left(\alpha - \frac{|\kappa|}{4} \right) \quad (4.23)$$

(see the Appendix). The upper boundaries of the four-fermion continuum for several values of Ω can be seen in Fig. 4 in comparison with the corresponding two-fermion continuum.

The four-fermion continuum always contains the two-fermion continuum. The lower boundaries coincide in part. The upper boundaries are different. In the zero field case we have $\omega_l = |J| \sin|\kappa|$ for both continua. The upper boundaries

are $\omega_u=4|J|\cos(\kappa/4)$ and $\omega_u=2|J|\sin(|\kappa|/2)$ for the two- and four-fermion continua, respectively. As the saturation field $\Omega=|J|$ is approached from below, the two-fermion continuum narrows to a branch and then disappears whereas the

four-fermion continuum remains an extended region, bounded by $\omega_l=4|J|\sin^2(\kappa/4)$ and $\omega_u=4|J|\cos^2(\kappa/4)$, and then disappears abruptly.

Now consider the equation

$$\sqrt{\sum_{j=1}^3 \left\{ \frac{\partial}{\partial \kappa_j} [\cos \kappa_1 + \cos \kappa_2 - \cos \kappa_3 - \cos(\kappa + \kappa_1 + \kappa_2 - \kappa_3)] \right\}^2} = 0. \quad (4.24)$$

It is satisfied for

$$\frac{\omega_s^{(1)}}{|J|} = 2 \sin \frac{|\kappa|}{2}, \quad (4.25)$$

$$\frac{\omega_s^{(2)}}{|J|} = 4 \sin \frac{|\kappa|}{4}, \quad (4.26)$$

$$\frac{\omega_s^{(3)}}{|J|} = 4 \cos \frac{\kappa}{4}. \quad (4.27)$$

Thus, for κ or ω approaching the curves (4.25)–(4.27) in (κ, ω) space, the quantity

$$\begin{aligned} S(\kappa, \omega) &= \int_{-\pi}^{\pi} d\kappa_1 \int_{-\pi}^{\pi} d\kappa_2 \int_{-\pi}^{\pi} d\kappa_3 S(\kappa_1, \kappa_2, \kappa_3, \kappa) \\ &\times \delta[\omega - |J|\cos \kappa_1 - |J|\cos \kappa_2 + |J|\cos \kappa_3 \\ &+ |J|\cos(\kappa + \kappa_1 + \kappa_2 - \kappa_3)] \end{aligned} \quad (4.28)$$

exhibits cusp singularities (akin to density-of-states effects in three dimensions). The exact nature of the cusps also depends on the factor $S(\kappa_1, \kappa_2, \kappa_3, \kappa)$, which varies between different dynamic structure factors with a four-fermion part. It always includes the factor $n_{\kappa_1} n_{\kappa_2} (1 - n_{\kappa_3}) (1 - n_{\kappa_1 + \kappa_2 - \kappa_3 + \kappa})$ as can be seen in expression (4.7). In Fig. 5 we show the ω dependence of $S(\kappa, \omega)$ as given by (4.28) at $\kappa = 0, \pi/2, 2\pi/3, \pi$ when $S(\kappa_1, \kappa_2, \kappa_3, \kappa) = 1$ and when $S(\kappa_1, \kappa_2, \kappa_3, \kappa) = n_{\kappa_1} n_{\kappa_2} (1 - n_{\kappa_3}) (1 - n_{\kappa_1 + \kappa_2 - \kappa_3 + \kappa})$ for several values of Ω .

At $T > 0$ the lower boundary of the four-fermion excitation continuum is smeared out and the upper boundary becomes $\omega_u = 4|J|\cos(\kappa/4)$.

The properties of the multimagnon continua of quantum spin chains have been examined in some detail in the recent paper of Barnes.²⁰ In particular, the lower and upper boundaries of the two- and higher-magnon continua were determined. It was shown that the boundary curves under certain conditions may exhibit discontinuous changes in composition and cusps. Moreover, a behavior of the density of (two- and higher-magnon) states on the continuum boundaries and within the continuum was considered and the existence of discontinuities was pointed out. These features of one-dimensional quantum spin systems are expected to become

accessible experimentally in high-resolution inelastic neutron scattering on alternating chain and ladder materials.

Interestingly, the $s=\frac{1}{2}$ transverse XX chain, which can be mapped onto noninteracting spinless fermions, provides an excellent example of a system whose dynamic properties are governed by continua of multifermion excitations. In particular, the dynamics of trimer fluctuations provides a direct mo-

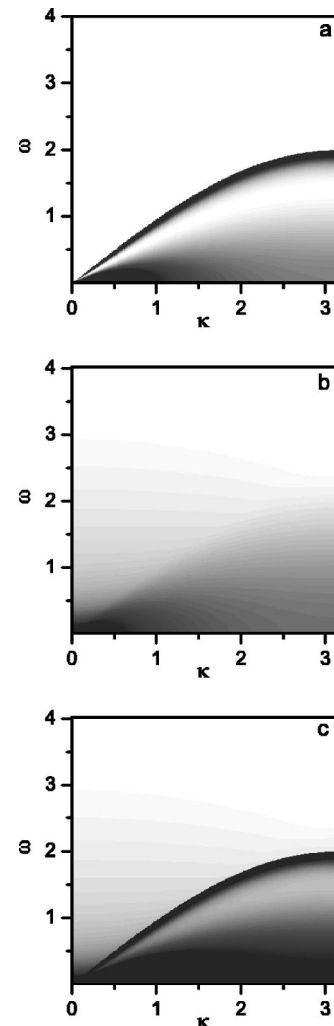


FIG. 10. $S_{TT}(\kappa, \omega)$ at $T \rightarrow \infty$ (independent of Ω ; only $\omega \geq 0$ is shown). Separate plots are shown for (a) $S_{TT}^{(2)}(\kappa, \omega)$, (b) $S_{TT}^{(4)}(\kappa, \omega)$, and (c) the sum $S_{TT}(\kappa, \omega)$.

tivation for analyzing the four-fermion excitation continuum. Unlike in the analysis reported in Ref. 20, where the statistics of the elementary excitations (magnons) is not known, here the quasiparticles are known to be fermions and the consequences are fully taken into account.

Finally, let us examine the explicit expression for the dynamic trimer structure factor $S_{TT}(\kappa, \omega)$ (4.5). In Figs. 6–9 we present the zero-temperature dynamic trimer structure factor at different values of Ω . In Fig. 10 we present the same quantity at infinite temperature. We show separately the two-fermion contribution (panels a in Figs. 6–10) and the four-fermion contribution (panels b in Figs. 6–10) as well as the sum of these contributions (panels c in Figs. 6–10). We observe how the spectral weight is spread across the four-fermion continuum. We also see that the two-fermion contribution stands out in terms of spectral weight. The two- and four-fermion contributions are comparable in intensity at $T=0$ and small Ω . As Ω increases the two-fermion contribution becomes more important and it completely dominates as $\Omega \rightarrow |J|$. In the high-temperature limit the two-fermion contribution is very dominant, but the four-fermion continuum is still in evidence.

V. CONCLUSIONS

In summary, we have investigated some aspects of the dynamics of the $s=\frac{1}{2}$ transverse XX chain, examining, in particular, the dynamics of dimer and trimer operators. For this purpose we have calculated several dynamic structure factors on a rigorous basis within the Jordan-Wigner representation. Although the dynamic dimer structure factor $S_{DD}(\kappa, \omega)$ and the dynamic transverse spin structure factor $S_{zz}(\kappa, \omega)$ are governed by fermionic one-particle-one-hole excitations, the dynamic trimer structure factor $S_{TT}(\kappa, \omega)$ also contains contributions from two-particle-two-hole excitations. We have described the structure of the two- and four-fermion excitation spectra in some detail and investigated the distribution of spectral weight in $S_{TT}(\kappa, \omega)$ across these continua at zero and nonzero temperature. In particular, we have established the boundaries of the four-fermion spectral range, the locations of soft modes, and the singularity structure, which in-

cludes one- and three-dimensional density-of-states features (van Hove singularities).

An alternative technique to evaluate dynamic structure factor of quantum spin chains is based on the Bethe ansatz solutions.^{5,16,17} Recently such an approach has been applied to the $s=\frac{1}{2}$ XX chain.¹⁶ Moreover, the relation between spinons or magnon quasiparticles and Jordan-Wigner fermions was discussed in some detail. It will be interesting to interpret the two- and four-fermion excitations discussed here in terms of the Bethe ansatz solution as studied in Ref. 16.

ACKNOWLEDGMENTS

This study was performed within the framework of the STCU Project No. 1673. O.D., J.S., and G.M. thank the Wilhelm und Else Heraeus-Stiftung for the kind hospitality during the 288. WE-Heraeus-Seminar on the Theme of “Quantum Magnetism: Microscopic Techniques for Novel States of Matter” (Bad Honnef, 2002) when the present study was launched. O.D. acknowledges the kind hospitality of the University of Dortmund in the spring of 2003 when part of the work was done. O.D. expresses gratitude to the Max-Planck-Institut für Physik Komplexer Systeme (Dresden) for its hospitality in the spring of 2004.

APPENDIX

To find the lower and upper boundaries of the four-fermion excitation continuum (4.8) at fixed Ω and $-\pi \leq \kappa \leq \pi$, we search for the extrema of $\omega/|J|$ as given in (4.8) and the values of $\kappa_1, \kappa_2, \kappa_3$, and κ_4 at which such extrema occur. Typical results are reported in Figs. 11 (lower boundary) and 12 (upper boundary).

In Fig. 11 we show the dependence on $|\kappa|$ of $\kappa_1, \kappa_2, \kappa_3$, and κ_4 , where $\omega/|J|$ assumes a local minimum. We distinguish five different regions. The global minimum yields the lower continuum boundary. If $0 \leq \kappa \leq \kappa_a$,

$$\kappa_1 = \alpha - \kappa, \quad \kappa_2 = \kappa_3 = \kappa_4 = \alpha \quad (\text{A1})$$

and

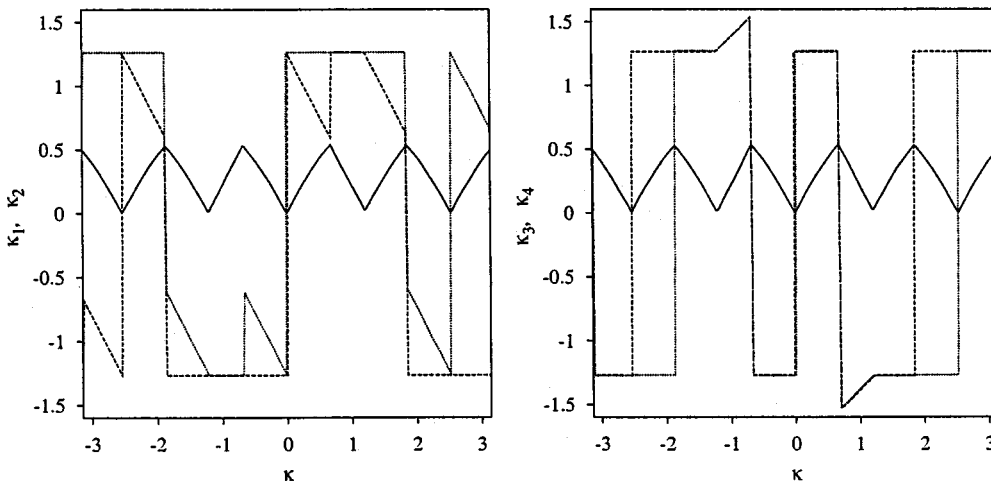


FIG. 11. Search for the lower boundary of the four-fermion excitation continuum. Shown are the values of $\kappa_1, \kappa_2, \kappa_3$, and κ_4 at which a minimum of $\omega/|J|$ as given in (4.8) occurs at $\Omega=0.3|J|$ and $-\pi \leq \kappa \leq \pi$. The dependences κ_1 and κ_3 on κ are shown by dashed curves, the dependences κ_2 and κ_4 on κ are shown by dotted curves, the dependence of the minimal value of $\omega/|J|$ on κ is shown by solid curves.

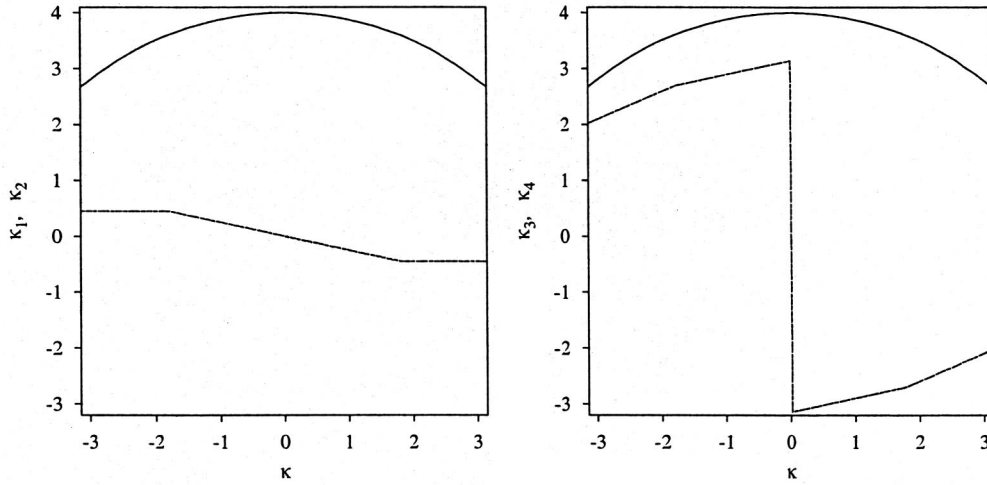


FIG. 12. Search for the upper boundary of the four-fermion excitation continuum. Shown are the values of κ_1 , κ_2 , κ_3 , and κ_4 at which a maximum of $\omega/|J|$ as given in (4.8) occurs at $\Omega=0.9|J|$ and $-\pi \leq \kappa \leq \pi$. The dependences of $\kappa_1(=\kappa_2)$ and $\kappa_3(=\kappa_4)$ on κ are shown by dashed curves, the dependence of the maximal value of $\omega/|J|$ on κ is shown by solid curves.

$$\frac{\omega_l}{|J|} = \cos(\alpha - \kappa) - \cos \alpha = 2 \sin \frac{\kappa}{2} \sin \left(\alpha - \frac{\kappa}{2} \right) = \frac{\omega_l^{(1)}}{|J|}; \quad \kappa_1 = \kappa_2 = -\frac{\kappa}{4}, \quad \kappa_3 = \kappa_4 = -\pi + \frac{\kappa}{4} \quad (\text{A2})$$

if $\kappa_a \leq \kappa \leq \kappa_b$,

$$\kappa_1 = \kappa_2 = \alpha, \quad \kappa_3 = \kappa_4 = \frac{\kappa}{2} + \alpha - \pi \quad (\text{A3}) \quad \frac{\omega_u}{|J|} = 4 \cos \frac{\kappa}{4} = \frac{\omega_u^{(1)}}{|J|}; \quad (\text{A6})$$

and

$$\frac{\omega_l}{|J|} = 2 \cos \alpha - 2 \cos \left(\frac{\kappa}{2} + \alpha - \pi \right) = 4 \cos \frac{\kappa}{4} \cos \left(\alpha + \frac{\kappa}{4} \right) = \frac{\omega_l^{(2)}}{|J|}, \quad (\text{A4})$$

if $\kappa_A \leq \kappa \leq \pi$,

$$\kappa_1 = \kappa_2 = -\alpha, \quad \kappa_3 = \kappa_4 = -\alpha - \pi + \frac{\kappa}{2} \quad (\text{A7})$$

and

$$\frac{\omega_u}{|J|} = 2 \cos \alpha + 2 \cos \left(\alpha - \frac{\kappa}{2} \right) = 4 \cos \frac{\kappa}{4} \cos \left(\alpha - \frac{\kappa}{4} \right) = \frac{\omega_u^{(2)}}{|J|}, \quad (\text{A8})$$

etc. The values of κ_a , κ_b , κ_c , and κ_d follow from the matching conditions.

In Fig. 12 we show the dependence on $|\kappa|$ of κ_1 , κ_2 , κ_3 , and κ_4 , where $\omega/|J|$ assumes a local maximum. We distinguish two different regions. The global maximum yields the upper continuum boundary. If $0 \leq \kappa \leq \kappa_A$,

etc. From the matching condition we find $\kappa_A = 4\alpha$.

*Corresponding author. Email address: derzhko@icmp.lviv.ua

¹V. S. Viswanath and G. Müller, *The Recursion Method: Application to Many-Body Dynamics* (Springer-Verlag, Berlin, 1994), and references therein.

²M. Takahashi, *Thermodynamics of One-Dimensional Solvable Models* (Cambridge University Press, Cambridge, UK, 1999).

³V. E. Korepin, N. M. Bogoliubov, and A. G. Izergin, *Quantum Inverse Scattering Method and Correlation Functions* (Cambridge University Press, Cambridge, UK, 1993).

⁴D. C. Mattis, *The Many-Body Problem: An Encyclopedia of Exactly Solved Models in One Dimension* (World Scientific, Singapore, 1993).

⁵G. Müller and M. Karbach, in *Frontiers of Neutron Scattering*, edited by A. Furrer (World Scientific, Singapore, 2000); arXiv: cond-mat/0003076.

⁶J. Lorenzana and G. A. Sawatzky, Phys. Rev. Lett. **74**, 1867 (1995); Phys. Rev. B **52**, 9576 (1995).

⁷H. Suzuura, H. Yasuhara, A. Furusaki, N. Nagaosa, and Y. Tokura, Phys. Rev. Lett. **76**, 2579 (1996).

⁸Yongmin Yu, G. Müller, and V. S. Viswanath, Phys. Rev. B **54**, 9242 (1996).

⁹J. Lorenzana and R. Eder, Phys. Rev. B **55**, R3358 (1997).

¹⁰R. Werner, Phys. Rev. B **63**, 174416 (2001).

¹¹E. Lieb, T. Schultz, and D. Mattis, Ann. Phys. (N.Y.) **16**, 407 (1961).

¹²S. Katsura, Phys. Rev. **127**, 1508 (1962); **129**, 2835 (1963).

¹³B. M. McCoy, E. Barouch, and D. B. Abraham, Phys. Rev. A **4**, 2331 (1971).

¹⁴G. Müller and R. E. Shrock, Phys. Rev. B **29**, 288 (1984).

¹⁵N. Kitanine, J. M. Maillet, and V. Terras, Nucl. Phys. B **554**, 647 (1999).

- ¹⁶D. Biegel, M. Karbach, G. Müller, and K. Wiele, Phys. Rev. B **69**, 174404 (2004).
- ¹⁷J. Sato, M. Shiroishi, and M. Takahashi, arXiv: cond-mat/0410102 (unpublished).
- ¹⁸G. Müller, H. Thomas, H. Beck, and J. C. Bonner, Phys. Rev. B **24**, 1429 (1981).
- ¹⁹J. H. Taylor and G. Müller, Physica A **130**, 1 (1985).
- ²⁰T. Barnes, Phys. Rev. B **67**, 024412 (2003).